energies

MDPI

Article

DC-Bus Voltage Sensorless Control of an Active Rectifier with Modular Multilevel Converter

Jianyu Pan [1,*], Yihao Du [1] and Ziwei Ke [2]

[1] School of Electrical Engineering, Chongqing University, Chongqing 400044, China; ld10061119@cqu.edu.cn
[2] School of Electrical Engineering, Guangdong University of Technology, Guangzhou 510006, China; ziweike@gdut.edu.cn
* Correspondence: panjianyu@cqu.edu.cn

Abstract: The modular multilevel converter (MMC) is recognized as one of the promising converters for the electrification of ships and railways. Among different energy conversion stages, the MMC-based rectifier should realize stable DC output voltage and accurate input current control. However, output DC-bus voltage sensors must be installed, which are costly and bulky. This paper presents a simple but effective control method for the MMC-based rectifier, removing the traditional output DC-bus voltage sensor. An accurate evaluation model of DC-bus voltage is developed as well as the implementing method. Meanwhile, a safe and fast pre-charging scheme is presented for the MMC-based rectifier without output voltage sensors. The fault-tolerant capability of the proposed method when the failure of the output DC-bus voltage sensor occurs is examined. Simulated and testing results demonstrate that the proposed method presents not only excellent steady-state and dynamic performance but also strong fault-tolerant capability. The proposed evaluation model for DC-bus voltage has a high accuracy with an error of less than 1%. Besides, the pre-charging time is less than 0.5 s using the proposed sensorless control.

Keywords: modular multilevel converter (MMC); active rectifier; sensorless control; capacitor pre-charging

Citation: Pan, J.; Du, Y.; Ke, Z. DC-Bus Voltage Sensorless Control of an Active Rectifier with Modular Multilevel Converter. *Energies* **2023**, *16*, 6569. https://doi.org/10.3390/en16186569

Academic Editor: Gianluca Brando

Received: 9 August 2023
Revised: 4 September 2023
Accepted: 5 September 2023
Published: 12 September 2023

1. Introduction

With the advancement of power electronics, modular multilevel converters (MMCs) are increasingly attractive solutions for all-electric ships and railway power supplies [1–3]. Compared with other converters, MMCs have salient features of modular structure, high efficiency, small line filter, and low-distortion grid current [4–6]. Figure 1 shows the corresponding structure of MMC-based converters in the application of railway power supply. They can be configured to perform ac/dc/ac conversion, which makes them suitable for the railway power grid at a different frequency (e.g., Europe 16.7 Hz at the locomotive side) [7,8].

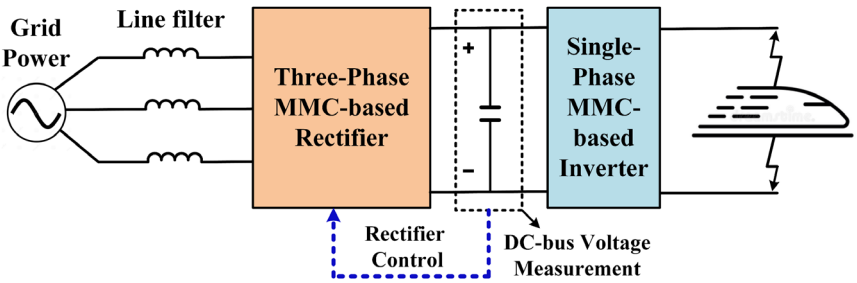

Figure 1. MMC-based converters for the railway power supply.

The MMC-based rectifier is the primary and critical stage for exchanging the energy between the AC grid and the medium-voltage DC bus. The DC-bus voltage and grid current must be strictly controlled to realize the desirable performance of the MMC-based rectifier [9,10]. For this purpose, the structure of rectifiers using MMC requires that the DC-bus voltage is communicated with the local and central controllers [8,11]. Voltage sensors are installed at the DC output side to obtain the feedback signal.

In recent years, a high-performance megawatt-scale MMC-based rectifier has been investigated to feed the medium-voltage DC system in the electric ship application [12]. It mainly focuses on hardware design and has good dynamic and fault-management performance. In addition, MMC-based rectifiers have been studied in the application of railway power supplies and HVDC systems [8,13–16]. Improved methods were proposed in aspects of circulating current suppression, voltage harmonic suppression, and capacitor voltage balancing. However, all those studies mentioned above require the output DC voltage to realize the accurate voltage and current control. In a real-world implementation, MMC-based rectifiers have output voltage levels from several to hundreds of kVs. In measuring those voltages, sensor devices must withstand high-voltage isolation and strong electromagnetic interference, which is costly and bulky [17,18]. For instance, a voltage sensor LV 200-AW/2/6400 from LEM (Geneva, Switzerland) measuring 6.4 kV voltage without partial discharge costs over USD 2000 [19]. The CHV-6-KV-10-KV voltage Hall sensor model from Beijing SENSOR Electronics Co., Ltd. (Beijing, China) costs over USD 1000 to measure 10 kV voltage [20]. Also, it will break the control of the active rectifier if a sensor fault occurs, inducing a reliability issue and a fatal system failure. The existing sensorless control of MMC mainly focuses on the online monitoring of capacitors. References [21,22] optimize the monitoring algorithm to eliminate the additional sensors required for traditional capacitor monitoring, and all these MMCs are used as inverters. There has been no research on the sensor optimization control method when MMC is used as a rectifier. Recognizing these challenges, this paper aims to develop a novel control strategy for the MMC-based rectifier that does not need a high-voltage DC-bus voltage sensor while maintaining effective control of the output voltage and grid current.

Moreover, the safe pre-charging scheme is another significant issue for MMC-based rectifiers if the DC-bus voltage sensor is removed [23]. Without proper control, submodule (SM) capacitors cannot be charged to the nominal value, and the inrush current threatens the MMC safety. The pre-charging process has been extensively studied in MMC DC/AC inverters. The conventional method uses limiting resistors and breakers placed on the input side or arms to charge SM capacitors [23,24]. Another effective way is to add an auxiliary low-voltage power supply and a blocking diode at the input DC side to charge capacitors [25]. However, those methods can only be applied to the MMC inverters. Authors in [26,27] presented the pre-charging method of the MMC-based rectifier with two-stage operation. However, both refs. [26,27] require the DC-bus voltage sensor to realize their methods, and the pre-charging process is complex.

This paper's major work and contribution are named as follows: (1) A simple but effective DC-bus voltage sensorless control strategy is proposed for MMC-based rectifiers. It takes advantage of the SM capacitor voltage inherent in each arm to evaluate the DC-bus output voltage, which aims to reduce costs and improve the performance of the rectifier. To determine the proper DC-bus voltage and minimize the estimated voltage ripples, an accurate evaluation model of DC-bus voltage is developed as well as a complete implementing method. (2) A closed-loop soft pre-charging scheme of the active MMC-based rectifier without a DC-bus voltage sensor is presented. It does not need any auxiliary power source and has only one stage to charge SM capacitors. (3) The fault-tolerant capability of the proposed method when the failure of the output DC-bus voltage sensor occurs is studied. A full-scale 4.16-kV/1-MVA simulation model and a down-scale MMC testbed are established to validate the effectiveness of the proposed method.

2. Circuit Configuration of MMC-Based Rectifier

Figure 2 shows the circuit structure of the MMC-based rectifier connected to a three-phase grid with the pre-charging circuit. There are two arms per phase of the main MMC circuit with each arm having a set of N-identical series-connected SMs and an inductor. The SM design on the MMC is carried out by a half-bridge power device due to its low cost and great control performance. In addition, SiC devices have been chosen as switching devices, which have higher voltage levels, operating frequencies, and temperatures compared to traditional Si devices.

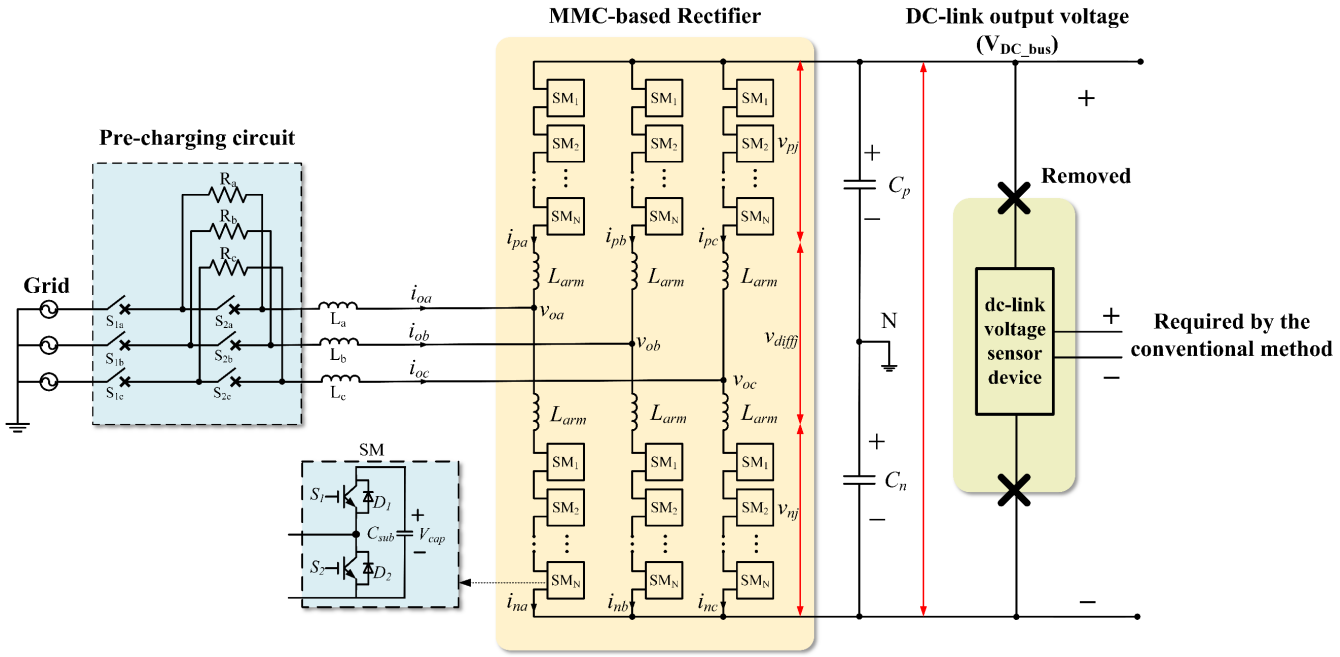

Figure 2. The circuit structure of the MMC-based rectifier with the pre-charging circuit.

For the input side, the pre-charging circuit and line filters (L_a, L_b, and L_c) connect the grid voltage to the MMC-based rectifier. The pre-charging circuit consists of limiting resistors (R_a, R_b, R_c), switches to connect/disconnect the grid source (S_{1a}, S_{1b}, S_{1c}), and switches to bypass/insert limiting resistors (S_{2a}, S_{2b}, S_{2c}). For the rectifier, v_{oj} ($j = a, b, c$) is the input voltage of phase j, while i_{oj} is the input current of the grid. In the following discussion, subscript j represents phases a, b, and c accordingly. The upper and lower arm voltages are expressed as v_{pj} and v_{nj}, where the subscript p and n indicate the upper (positive) and lower (negative) arms, respectively. The upper arm, lower arm, and circulating currents of phase j are i_{pj}, i_{nj}, and i_{diffj}, respectively. v_{diffj} is the voltage difference between the DC-bus voltage and the total inserted capacitor voltage in phase j. The inductance of the arm is L_{arm}. C_{sub} is the SM capacitance and V_{cap} is the rated voltage of the capacitor. C_p and C_n represent the upper and lower arm capacitors connected to the DC-bus.

The output of the rectifier ($V_{DC\text{-}bus}$) supplies the load or the DC grid. A high-voltage sensor device is generally installed on traditional active rectifiers to measure the DC-bus output voltage. It is needed for the feedback signals of the active rectifier control. However, the proposed method removes the DC-bus voltage sensor. It reduces the cost and volume of the system. Also, removing the sensor avoids system operational issues caused by its failure which increases system fault tolerance. This improves the reliability of the MMC system.

The relationships between current and voltage in the MMC are given in Equations (1)–(6) [4–6]:

$$i_{oj} = i_{pj} - i_{nj} \tag{1}$$

$$i_{pj} = i_{diffj} + \frac{1}{2} i_{oj} \tag{2}$$

$$i_{nj} = i_{diffj} - \frac{1}{2} i_{oj} \tag{3}$$

$$i_{diffj} = \frac{i_{pj} + i_{nj}}{2} \tag{4}$$

$$v_{oj} = \frac{v_{nj} - v_{pj}}{2} - \frac{1}{2} L_{arm} \frac{di_{oj}}{dt} \tag{5}$$

$$\begin{aligned} V_{DC\_bus} &= v_{diffj} + v_{pj} + v_{nj} \\ &= L_{arm}\left(\frac{di_{pj}}{dt} + \frac{di_{nj}}{dt}\right) + (v_{pj} + v_{nj}) \\ &= 2L_{arm} \frac{di_{diffj}}{dt} + (v_{pj} + v_{nj}) \end{aligned} \tag{6}$$

Based on Equations (1)–(6), the MMC output voltage is controlled by the difference of upper and lower arm voltages, while the circulating current i_{diffj} is governed by the sum of upper and lower arm voltages.

3. Proposed Control Method

The MMC consists of a group of SMs in each phase, which is different from the traditional 2- or 3-level inverters. For normal operation, each SM is equipped with an inherent voltage sensor to measure the capacitor voltages. The output DC-bus voltage can be estimated with the information of SM capacitor voltages and therefore the high-voltage sensor at the output side can be removed. However, without a proper algorithm, the SM capacitor voltage ripples affect the accuracy of estimation to the output DC-bus voltage. The harmonics of grid current could be large, and the performance of the MMC-based rectifier is poor.

Eliminating the DC-bus voltage sensors is the principal objective of all estimation methods while maintaining good accuracy. Given the impact of SM capacitor voltage fluctuations and signal interference on the output voltage, all three-phase capacitor voltages should be considered to reduce voltage fluctuations and to achieve a stable DC voltage V_{eva}.

A simple but accurate evaluation algorithm to obtain the DC-bus output voltage is developed from (7) to (10):

$$V_{ave_a} = \sum_{i=1}^{2N} V_{cap_{a(i)}} / 2N \tag{7}$$

$$V_{ave_b} = \sum_{j=1}^{2N} V_{cap_{b(j)}} / 2N \tag{8}$$

$$V_{ave_c} = \sum_{j=1}^{2N} V_{cap_{c(j)}} / 2N \tag{9}$$

$$V_{eva} \approx \frac{(V_{ave_a} + V_{ave_b} + V_{ave_c})}{3} \cdot N \approx \frac{\sum_{j=1}^{2N} V_{cap_{a(j)}} + \sum_{j=1}^{2N} V_{cap_{b(j)}} + \sum_{j=1}^{2N} V_{cap_{c(j)}}}{6} \tag{10}$$

where, the jth SM capacitor voltage of phases a, b, and c is represented by $Vcap_{a(j)}$, $Vcap_{b(j)}$, and $Vcap_{b(j)}$. N is the SM number for each arm. $Vave_a$, $Vave_b$, and $Vave_c$ are the averaged values of capacitor voltages of phases a, b, and c respectively. V_{eva} is the evaluated value of the output DC-bus voltage. Fluctuation components of capacitor voltages are minimized by using this algorithm. The voltage sensor at the output side is no longer needed.

The sampling frequency of capacitor voltage typically exceeds kHz. The high-frequency noise could appear on the evaluated value of $V_{DC\text{-}bus}$, leading to unacceptable harmonics at the grid currents. Therefore, the high-frequency noise of $V_{DC\text{-}bus}$ reduction also requires a filter algorithm. A straightforward filter algorithm is shown as (11):

$$V_{eva\_filter} = \sum_{j=1}^{M} V_{pre(j)} / M \tag{11}$$

where, V_{eva_filter} is the final evaluated value of $V_{DC\text{-}bus}$, which removes the high-frequency component noise. $V_{eva(j)}$ is the evaluated value of $V_{DC\text{-}bus}$ at the jth constant, and M represents the sampling count for a long period. The sampling frequency of voltage sensors used in SM capacitors is 10 kHz which can be easily realized by the real-world voltage sensor. Therefore, the sampling frequency in the simulation and experimental validation is chosen at 10 kHz to maintain consistency. Additionally, too large values of M significantly affect the dynamic response of the prediction, leading to poor control response of the system and M was suggested as 5–15 to ensure good estimation accuracy. The value of M was chosen as 10 in the simulation and experiment in Sections 4 and 5.

Figure 3 shows the sensorless control block diagram of the MMC-based rectifier, which consists of the evaluation algorithm, output voltage closed-loop control, active and reactive current decoupled control, and MMC arm voltage control. The evaluation algorithm is used to replace the traditional feedback signal from the high-voltage sensor device on the DC output side, which is based on Formulas (7)–(11). A proportional–integral (PI) controller is used to make the output voltage follow its reference value. To realize the decoupled control of the active and reactive power of the MMC-based rectifier, a modified current vector control is applied, which can accurately regulate the active/reactive current magnitude and angle. The detailed principle of the modified current vector is shown as follows.

To achieve decoupled control of the output current, two closed-loop controllers with PI are applied to the d-axis and q-axis current, respectively. The parameters of the d–q axis current corresponding to the PI controller are K_p and K_i, respectively. To be noted, d- and q-axis components of grid voltage are considered in the control loop, which are v_{gd} and v_{gq}, respectively. They are added to the output voltage references. $v_{d.ref}$ and $v_{q.ref}$ represent the d-axis and q-axis references, which are defined by (12) and (13):

$$v_{d.ref} = v_{gd} + (K_p + \frac{K_i}{s})(i_{d.ref} - i_d) + \omega L_o i_q \tag{12}$$

$$v_{q.ref} = v_{gq} + (K_p + \frac{K_i}{s})(i_{q.ref} - i_q) - \omega L_o i_d \tag{13}$$

where i_d and i_q are the d- and q-axis components of the i_{oj}. $i_{d.ref}$ and $i_{q.ref}$ represent the d-axis and q-axis current references. L_o is the filter inductance, and ω is the grid angular frequency. The last component in (12) and (13) is negligible since the filter inductance is small in the MMC-based rectifier.

Based on the control diagram, the active and reactive power of the MMC-based rectifier can be calculated as (14) and (15). The phase voltage phase degree is 0 when the system is in a three-phase balanced steady-state with $v_{gq} = 0$. In return, the d-axis and q-axis current references can also be obtained if the designed active and reactive power are known:

$$P = \frac{3}{2}(v_{gd} i_d + v_{gq} i_q) = \frac{3}{2} v_{gd} i_d \tag{14}$$

$$Q = \frac{3}{2}(v_{gq} i_d - v_{gd} i_q) = -\frac{3}{2} v_{gd} i_q \tag{15}$$

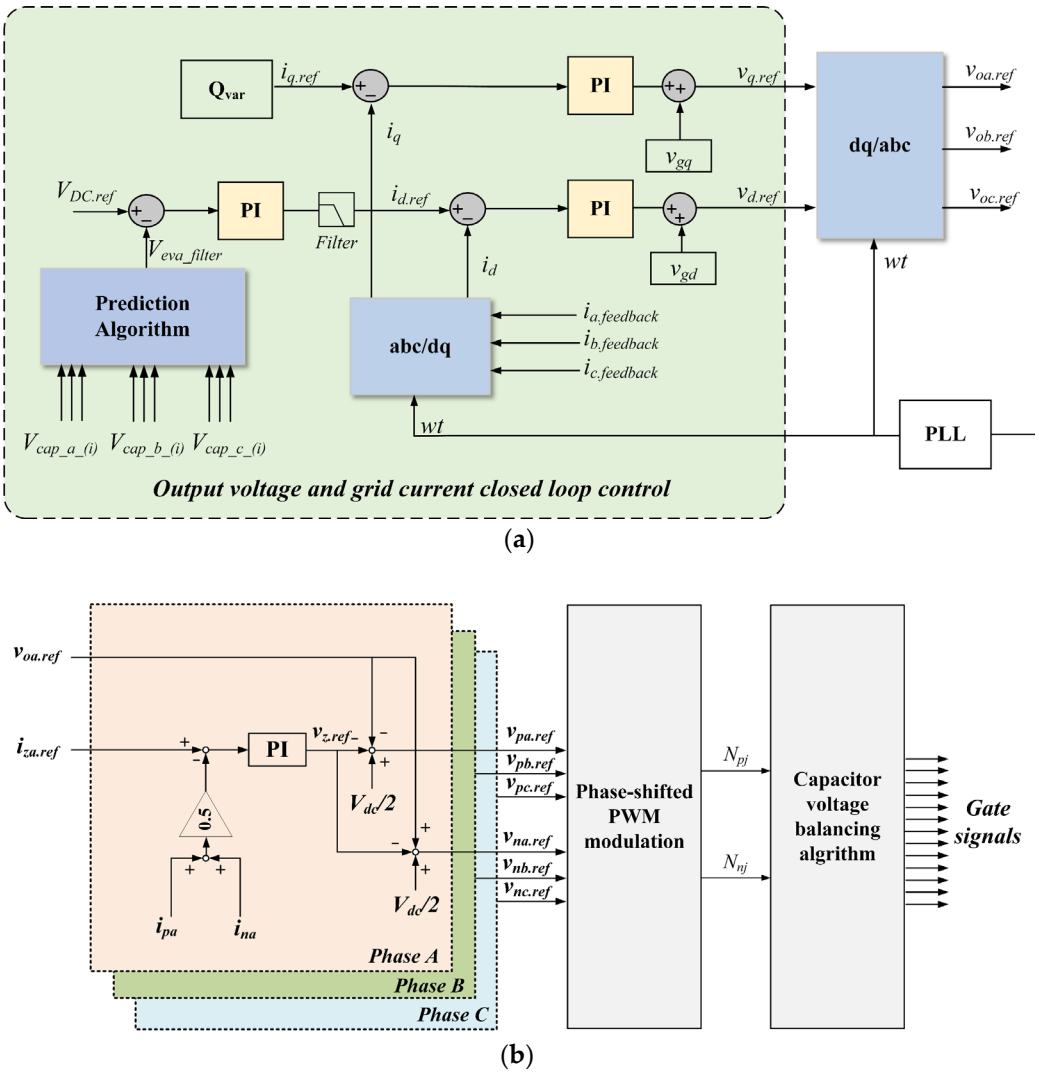

Figure 3. Sensorless control block diagram of the MMC-based rectifier. (**a**) Output DC-bus voltage and grid current closed-loop control. (**b**) MMC arm voltage generation and modulation control.

When the output DC-bus voltage sensor is removed, the pre-charging of the MMC-based rectifier becomes a major issue. Without proper control, inrush currents could be induced, and capacitor voltage could fail to reach the rated value. This paper further develops an effective closed-loop pre-charging scheme for the MMC-based rectifier without the output DC-bus voltage measurement. Compared with existing pre-charging methods of MMCs in [26,27], the proposed method safely charges the MMC from the AC source. It only needs a one-stage operation, and the MMC-based rectifier automatically enters the closed-loop control of the grid current and the capacitor voltage.

A closed-loop soft pre-charging scheme is shown in Figure 4. The pre-charging scheme has five steps, which are described as follows:

Step 1: All switches are turned off in Figure 2. The MMC-based rectifier is not connected to the power grid before the pre-charging process. The SM capacitor voltage and output dc-bus voltage are zero. The limiting resistor (R_j) is inserted by controlling the switch (S_{2j}) to the off state.

Step 2: The proposed control method is applied to the MMC-based rectifier. The output DC-bus voltage is set to $V_{DC.ref}$. The reactive current reference in the q-axis is set to 0. An upper boundary value is applied to the d-axis current reference to suppress the charging current.

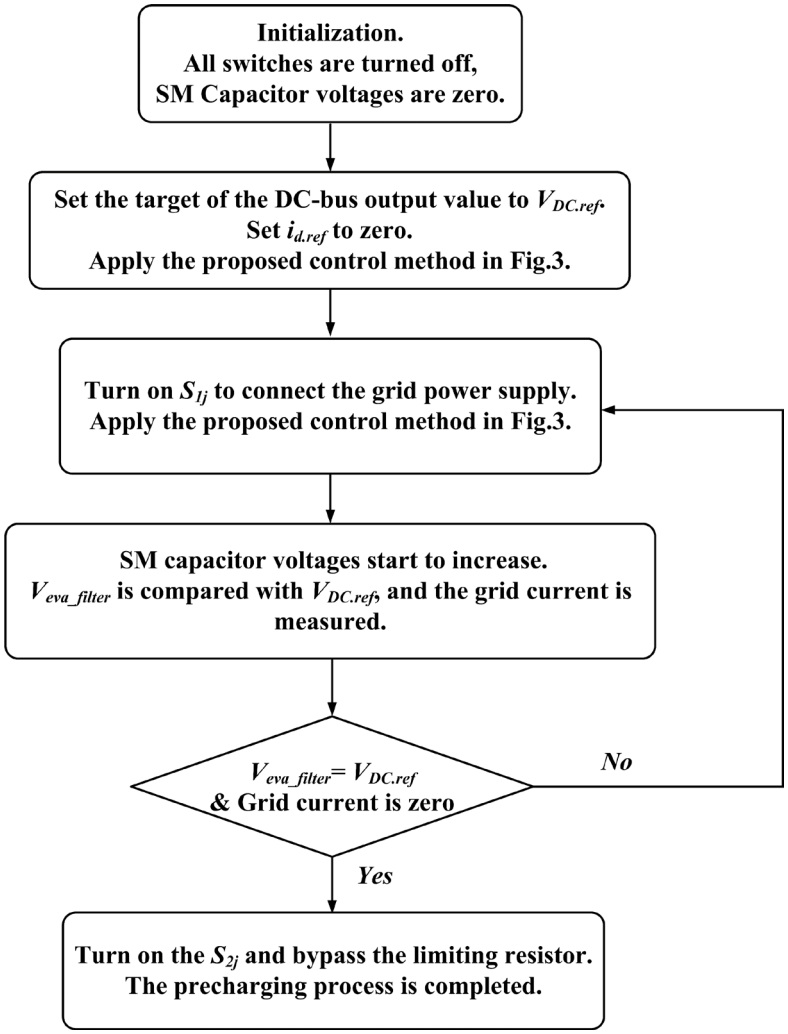

Figure 4. The closed-loop pre-charging scheme of the MMC-based rectifier without output DC-bus voltage sensors.

Step 3: Switches S_{1j} are turned on. The AC current flows from the grid source through the limiting resistor R_j and charges the SM capacitors. The maximum charging current is suppressed due to the limiting resistor.

Step 4: SM capacitor voltages are simultaneously increasing. All capacitor voltages and grid currents are measured. If the calculated output DC-bus voltage V_{eva_filter} with the proposed method is equal to $V_{DC.ref}$ and the charging current is reduced to zero, the pre-charging process goes to the next step. Otherwise, it will repeat steps 3 and 4.

Step 5: Switches S_{2j} are turned on, and the limiting resistors are bypassed. The MMC-based rectifier is connected to the grid. The pre-charging process is completed. The MMC-based rectifier is waiting for further control commands.

4. Simulation Analysis

To verify the proposed control method, a simulation model for a 7-level MMC-based rectifier with a 4160 V/60 Hz grid voltage is established in MATLAB/Simulink (2022b). The specific simulation parameters are shown in Table 1. In the MMC, each arm has 6 SMs and the SM capacitor is chosen as 0.62 mF. The arm inductor is 0.13 mH. The limiting resistor is 50 Ω, and the line filter is 1.7 mH. The target of the output DC-bus voltage is 7200 V.

Table 1. Parameters of the MMC-based rectifier.

Parameter	Description	Simulated Value	Experimental Value
V_{grid} (V)	Grid line-line voltage	4160	400
$V_{DC\text{-}bus}$ (V)	Rated output DC-bus voltage	7200	1000
N	Number of SMs per arm	6	2
C (mF)	SM capacitance	0.62	0.62
V_{cap} (V)	Rated SM capacitor voltage	1200	500
L_{arm} (mH)	Arm inductance	0.15	0.15
f_c (kHz)	Carrier frequency	4	12
f_b (Hz)	Rated frequency	60	60

4.1. Pre-Charging Control Mode

Figure 5a,b shows the closed-loop control results of the MMC-based rectifier during the pre-charging process. In the beginning, all SM capacitor voltages are not charged, and the charging resistors are inserted. The output DC-bus voltage is zero. When the proposed sensorless method is enabled and the MMC-based rectifier is connected to the grid power supply, the output DC-bus voltage is successfully controlled to the target value (7200 V) within 0.35 s. The capacitor voltages are gradually increased to the nominal voltage. Then the charging resistor is bypassed. There are no inrush currents to the grid current and arm current. The output voltage stabilizes very well at 7200 V, and a 7-level staircase arm voltage is observed. Thus, the results of Figure 5 validate that the proposed method effectively controls the DC-bus output voltage to the required value without output DC-bus voltage sensors. The full pre-charging process is safe and rapid for the MMC-based rectifier.

4.2. Active and Reactive Power Control Mode

The performance of the active power/current control when the DC-bus voltage sensor is removed is evaluated in Figure 6. A large active load (0.5 MW) is intentionally added on the output side, corresponding to 100 A grid current at t = 0.45 s. It can be observed that the grid current is in phase with the grid voltage and presents high-quality sinusoidal waveforms. When the active load is added, the DC-bus voltage still stabilizes at approximately 7200 V. In addition, the DC-bus current is increased from 0 to 74 A. The fluctuation of capacitor voltage is slight, within 5%, and a high-quality arm voltage is generated. It can be verified that the proposed sensorless method has accurate control of the active current and output DC-bus voltage. Also, a strong dynamic stabilizing capability is observed.

The performance of reactive power/current control is investigated in Figure 7. A large reactive load (0.5 MVar) is added at 0.45 s. The reactive power corresponding to 100 A current circulates between the grid and the MMC-based rectifier, thus not going to the output side. The results show that the grid current is controlled with 90° lag of the grid voltage with a high-quality waveshape. The output DC-bus voltage is stable at 7200 V with minor variations. The fluctuation of SM capacitor voltage is within ±10% in p.u. During the transient, all the arm currents and voltage are in good shape. Thus, the proposed sensorless control method can control the active and reactive power of the MMC-based rectifier independently, with high-quality grid current and strong dynamic-stabilizing capability.

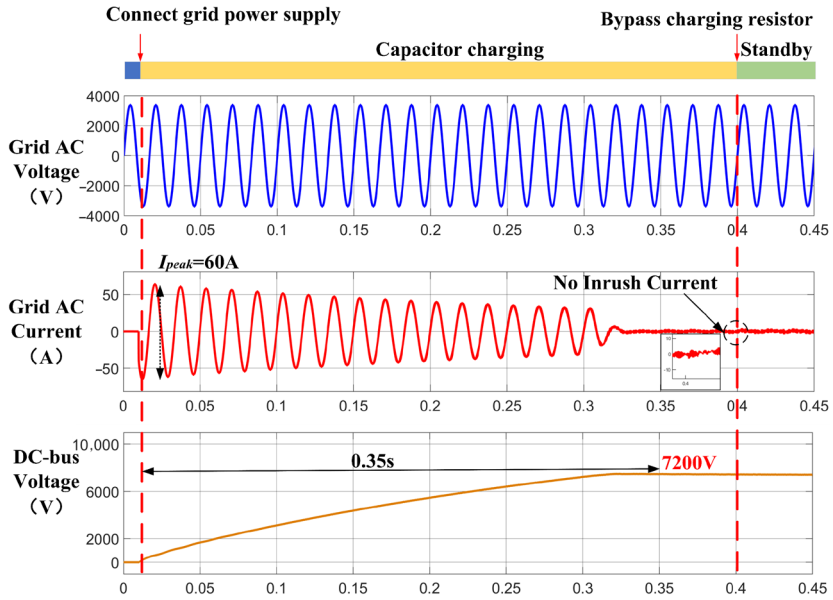

(**a**)

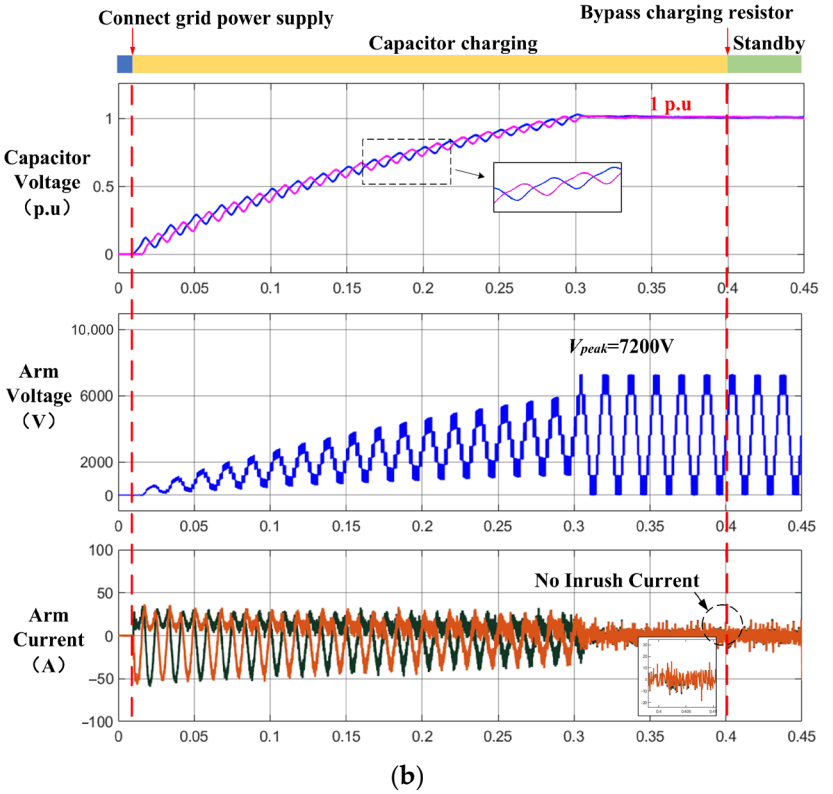

(**b**)

Figure 5. Simulation results for the pre-charging process of the MMC-based rectifier. (**a**) Grid voltage, grid current, output DC-bus voltage. (**b**) Capacitor voltage in p.u., arm voltage, upper and lower arm current.

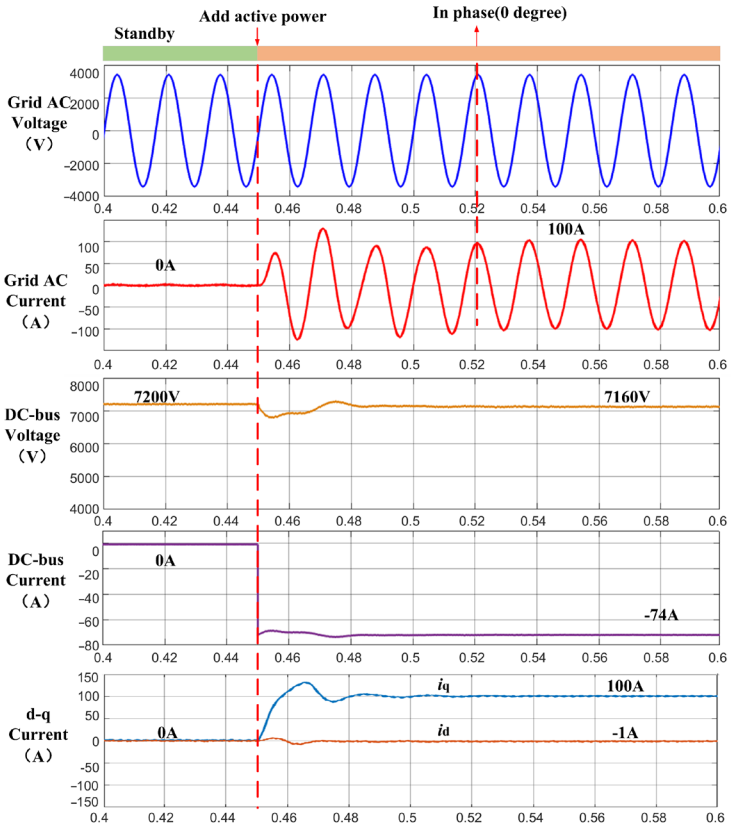

(**a**)

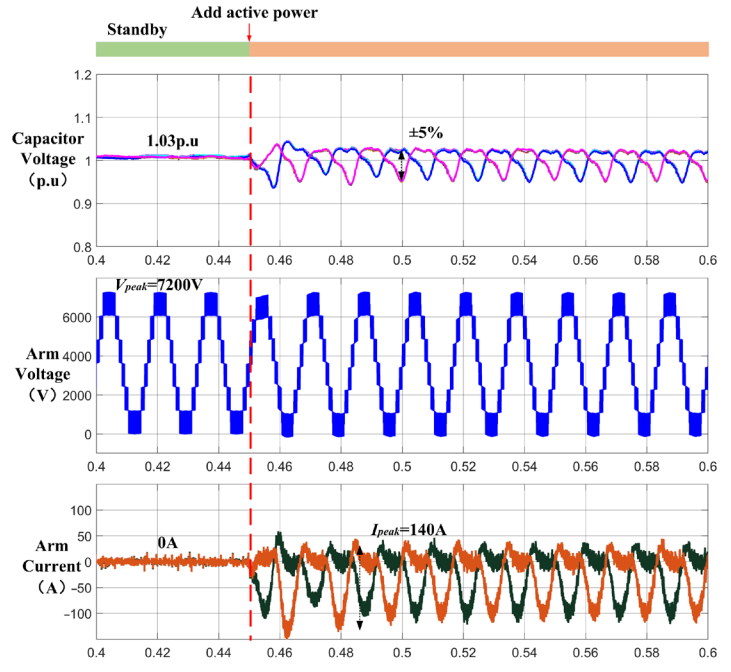

(**b**)

Figure 6. Simulation results of active power control at dynamic conditions. (**a**) Grid voltage, grid current, output DC-bus voltage and current, *d*-*q* current. (**b**) Capacitor voltage in p.u, arm voltage, upper and lower arm current.

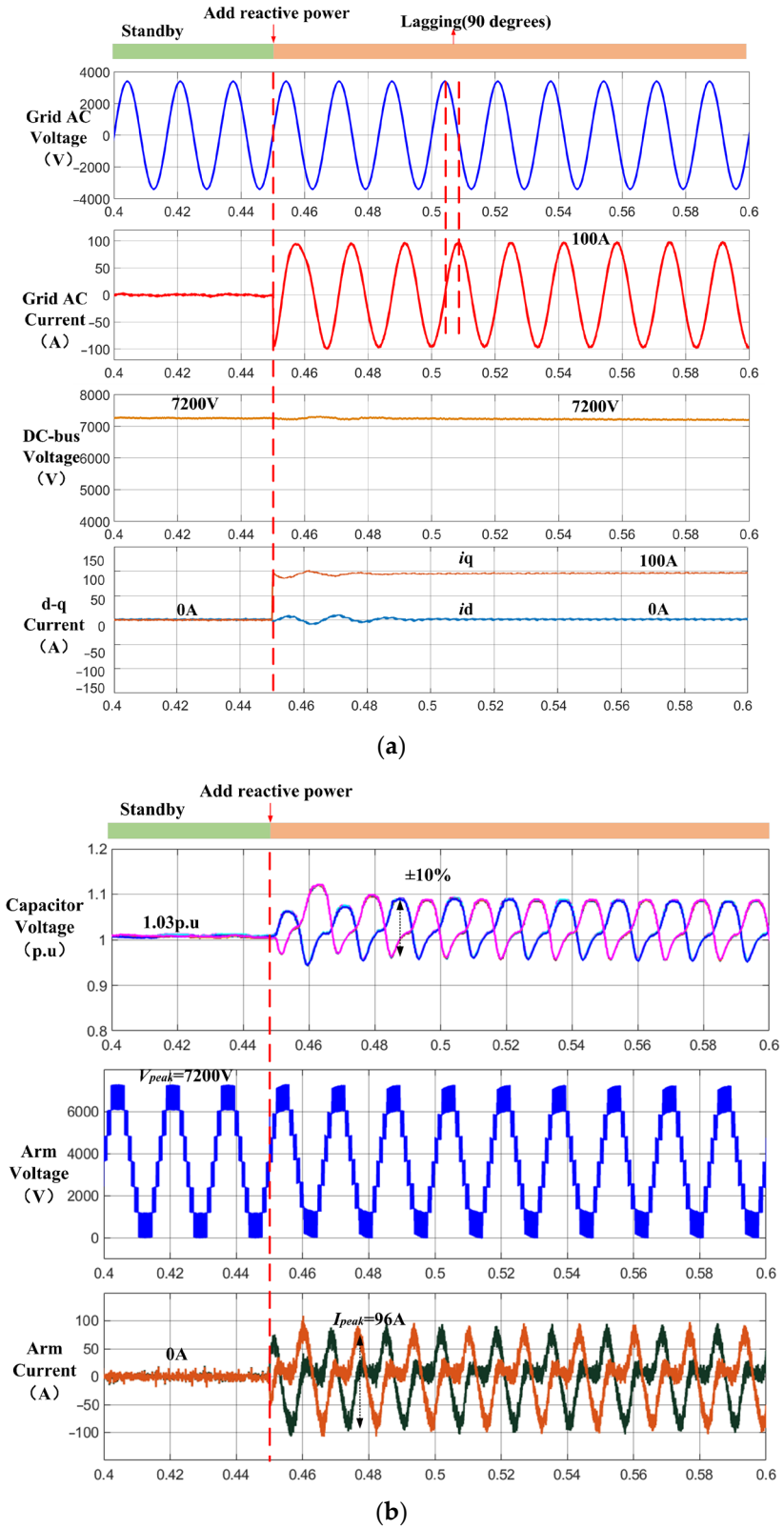

Figure 7. Simulation results of reactive power control at dynamic conditions. (**a**) Grid voltage, grid current, output DC-bus voltage, *d*-*q* current. (**b**) Capacitor voltage in p.u, arm voltage, upper and lower arm current.

To further investigate the performance of grid currents with the proposed method, the fast Fourier transform (FFT) is examined in Figure 8. The calculated total harmonic

distortions (THDs) for the grid current during the active and reactive power mode are 1.38% and 1.55%, respectively. Thus, FFT results demonstrate the proposed method has accurate control of the grid current with extra-low harmonics when the DC-bus voltage sensor is removed.

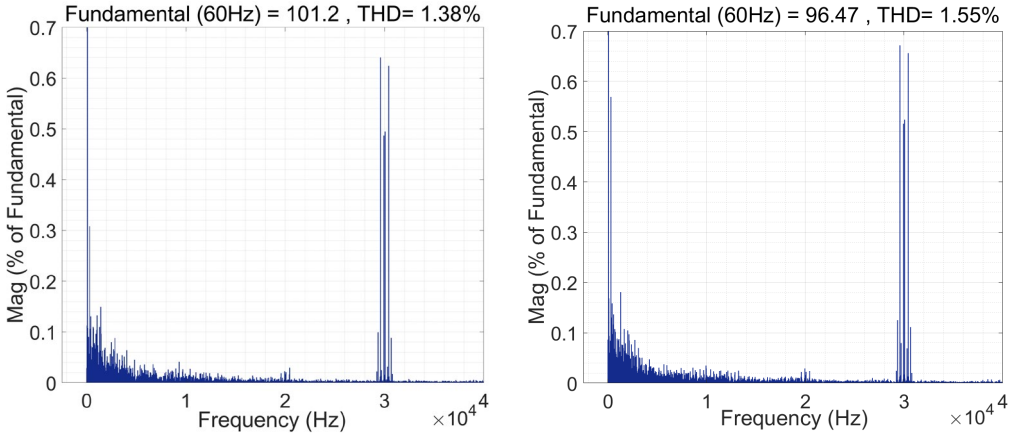

(**a**) (**b**)

Figure 8. FFT analysis of the grid current. (**a**) Current THD% during the active power mode. (**b**) Current THD% during the reactive power mode.

4.3. Output DC-Bus Voltage Control and Fault Mode

The response of the DC-bus voltage control of the proposed sensorless method is evaluated in Figure 9. The DC-bus voltage is intentionally increased to 10,000 V (+35%) and back to 7200 V. The increase/decrease rate is approximately 17 kV/s. Figure 9 demonstrates that the proposed sensorless method can effectively control the output DC-bus voltage to 10,000 V and back to 7200 V. The capacitor voltages can be charged to the 1.4 p.u voltage at the same time. The entire control process is almost symmetrical between the charging and discharging processes. No instability issues were observed. To be noted, the bidirectional current control is realized during this process. Thus, the results in Figure 8 firmly validate that the proposed sensorless method has a strong control capability of adjusting output DC-bus voltage over a wide range.

To highlight the advantages of the proposed sensorless control method, the high-voltage sensor fault was intentionally created and studied for the MMC-based rectifier. Initially, the rectifier was controlled with the conventional method using the correct feedback signal from high-voltage sensors on the output DC-bus side. Then the sensor fault occurred at 0.6 s, and the proposed sensorless control method was enabled at 0.8 s.

Figure 10 shows that the output DC-bus voltage lost control at 0.6 s when the sensor fault occurred for the conventional method. The DC-bus voltage is dramatically increased to 13,000 V, with distorted arm voltage and surged capacitor voltage (190%). When the sensor fails, the voltage difference between $V_{DC.ref}$ and $V_{DC\text{-}bus}$ becomes excessively large. The DC-bus voltage continues charging until it reaches the upper limit voltage $V_{DC.lim}$ = 13,000 V. Consequently, it could quickly burn the devices and cause a fatal system failure. When the proposed method is enabled, the DC-bus voltage recovers to 7200 V quickly (in 0.1 s). The capacitor voltage stabilizes at the nominal value, and the arm voltage is well-regulated. Thus, the proposed method can enable the MMC-based rectifier to survive and function well even if the output DC-bus voltage sensor fails. It has a robust fault-tolerant capability for the output DC-bus voltage sensors.

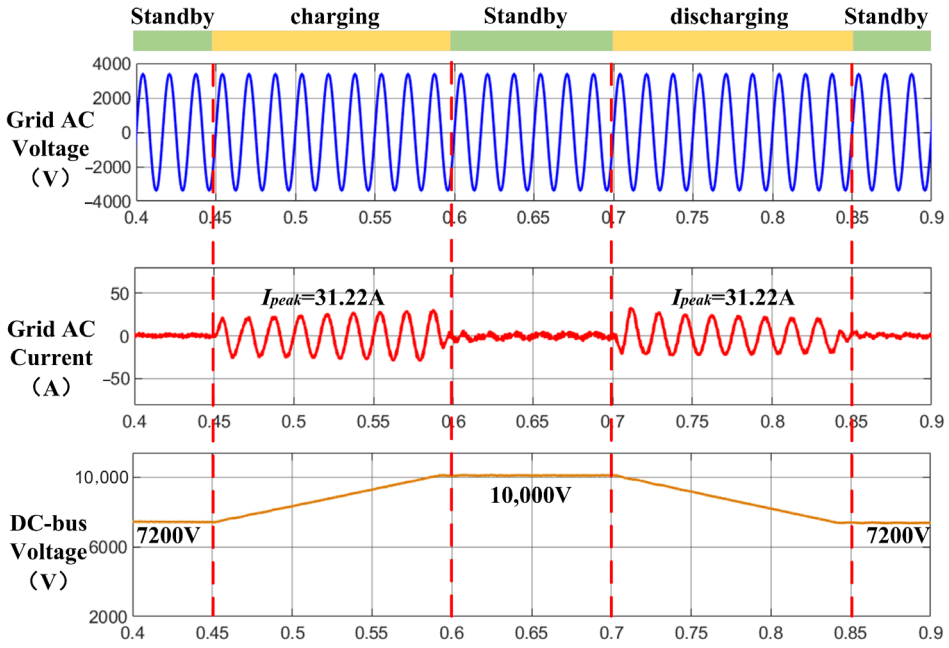

(**a**)

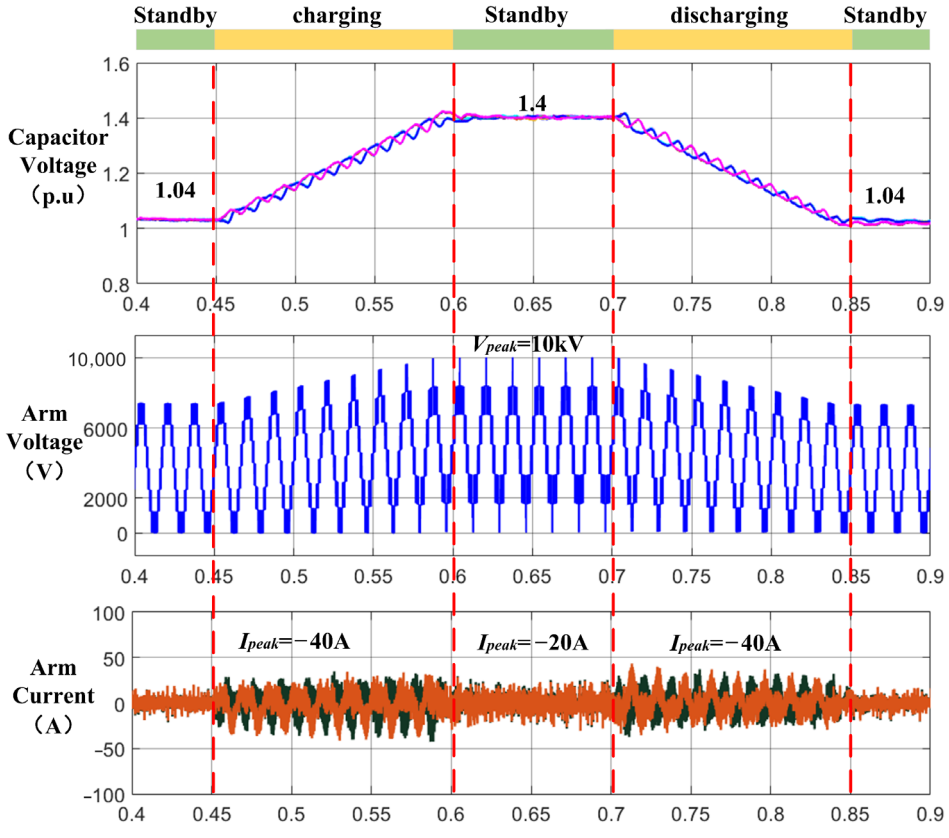

(**b**)

Figure 9. Simulation results of the output DC-bus voltage control from 7400 V to 10,000 V. (**a**) Grid voltage, grid current, output DC-bus voltage. (**b**) Capacitor voltage in p.u., arm voltage, upper and lower arm current.

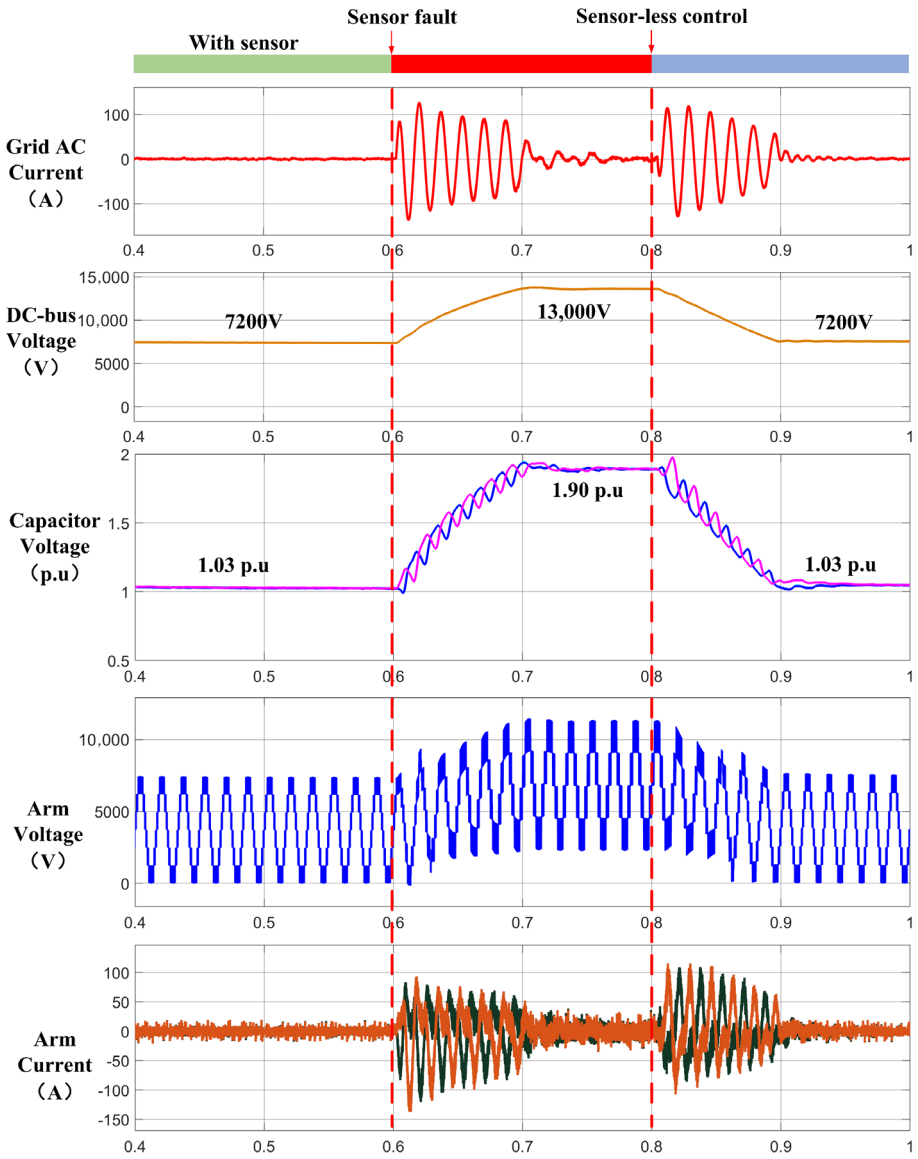

Figure 10. Simulation results of the conventional method to sensor-less control method in the fault mode. Grid current, DC-bus voltage, capacitor voltage in p.u., arm voltage, upper and lower current.

5. Experimental Results

5.1. Experimental Test Platform

The proposed sensorless control method for the MMC-based rectifier was also examined on an MMC experimental prototype, which is shown in Figure 11. Detailed parameters of the MMC-rectifier test platform are shown in Table 1. Each arm has two SMs with an SM capacitance of 0.62 mF. Each SM employs a BSM250D17P2E004 SiC half-bridge power module produced by ROHM Semiconductor (Kyoto, Japan). The DSP TMS320F28379D produced by Texas Instruments Incorporated (Dallas, TX, USA) and FPGA Cyclone IV EP4CE40F29C8N produced by Terasic Technologies (Taiwan, China) controllers were used to implement the proposed method. No voltage sensors are installed on the output side of the MMC-based rectifier as feedback signals. Various conditions were tested to validate the effectiveness of the proposed sensorless control method of the MMC-based rectifier.

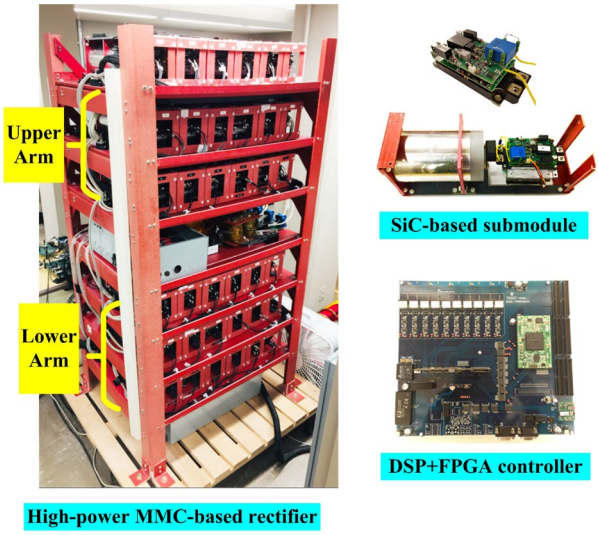

Figure 11. MMC-based rectifier testbench with SiC devices.

5.2. Testing Results

The pre-charging process of the proposed method for the MMC-based rectifier is examined in Figure 12. In Figure 12, the positive direction of current is from the rectifier to the AC grid. The initial capacitor voltage and output voltage are zero. The desired DC output voltage is set at 1000 V, with the corresponding capacitor voltage of 500 V. The limiting resistor is 10 Ω, and the grid voltage amplitude is 400 V. The proposed sensorless methodology is enabled and therefore the MMC-rectifier is connected to the grid power. The curves from top to bottom are the grid voltage, grid current, arm voltage, DC-bus voltage, and upper and lower capacitor voltages.

Figure 12 shows that (1) the output DC-bus voltage is successfully controlled and stabilized at 1000 V within 220 ms; (2) the capacitor voltages are gradually increased to 500 V during the same period; (3) the maximum grid current is kept below 50 A and goes to zero when the capacitor voltages are fully charged. The experimental results in Figure 12 comply very well with the simulation analysis of the methodology. The proposed sensorless control method can charge the MMC-based rectifier safely and rapidly with controllable output DC-bus voltage and limited charging current.

Given the lack of a large active load in the laboratory, the DC-bus voltage was controlled at 600 V in subsequent experiments. The grid line-line voltage is 240 V in RMS. To demonstrate the effectiveness of the proposed method, the performance of the MMC was tested in both reactive and active power control modes. The grid current is 40 A in amplitude. Two conditions were considered for the steady-state reactive power/current control mode: the grid current leads the voltage (leading mode) and the grid current lags the voltage (lagging mode), as shown in Figures 13 and 14. In Figures 13–16, the positive direction of the current is from the AC grid to the rectifier.

Results show that both modes control the output DC-bus voltage at 600 V. During the leading mode, the grid voltage precisely leads the current by 90 degrees, while the grid voltage lags the current by 90 degrees during the lagging mode. The grid currents present a high-quality sinusoidal waveshape. Meanwhile, the capacitor voltages are all maintained around 300 V with small voltage fluctuations of less than 6%. The leading and lagging modes imply that the MMC-based rectifier can generate or absorb reactive power interchange with the grid source. Thus, the proposed sensorless method presents accurate and stable reactive power/current control for the MMC-based rectifier.

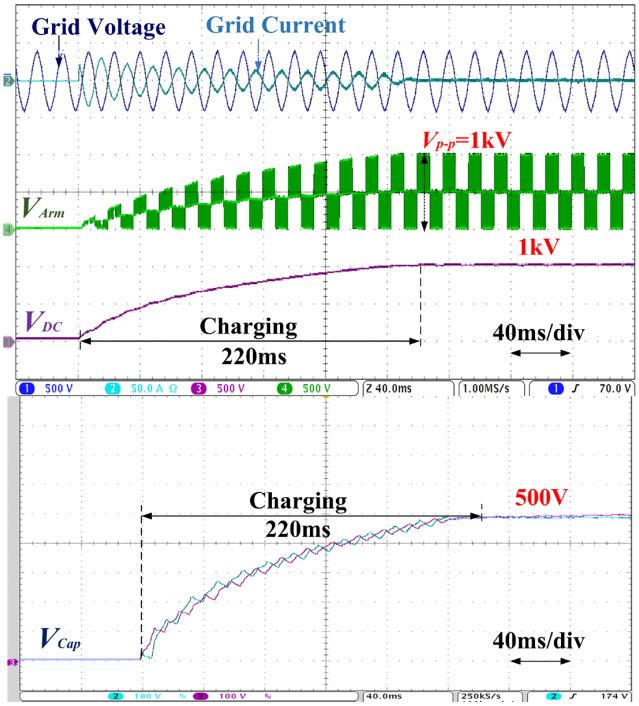

Figure 12. Experimental results of the pre-charging process of the MMC-based rectifier: the grid voltage (500 V/div), grid current (50 A/div), arm voltage (500 V/div), DC-bus voltage (500 V/div) and capacitor voltage (100 V/div, from **top** to **bottom**).

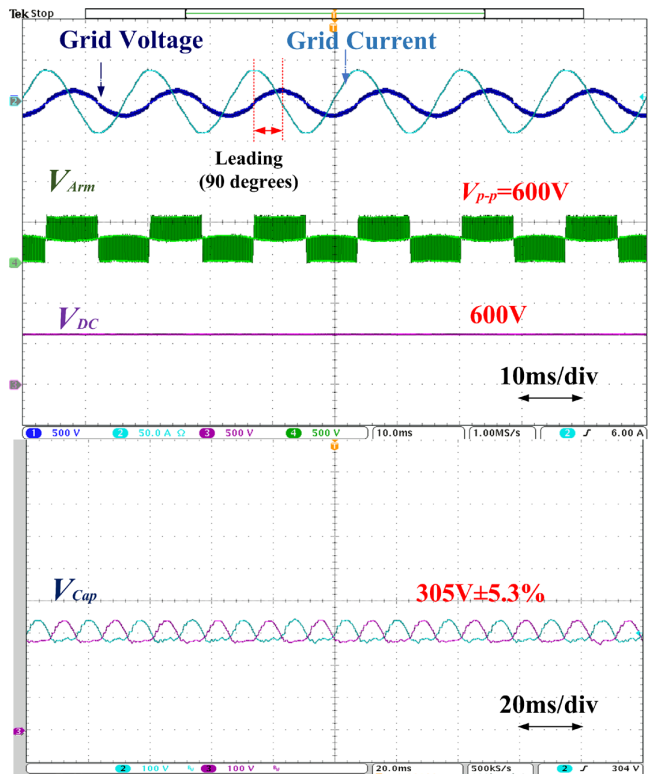

Figure 13. Experimental results of the reactive power/current control in the leading mode: the grid voltage (500 V/div), grid current (50 A/div), arm voltage (500 V/div), DC-bus voltage (500 V/div) and capacitor voltage (100 V/div, from **top** to **bottom**).

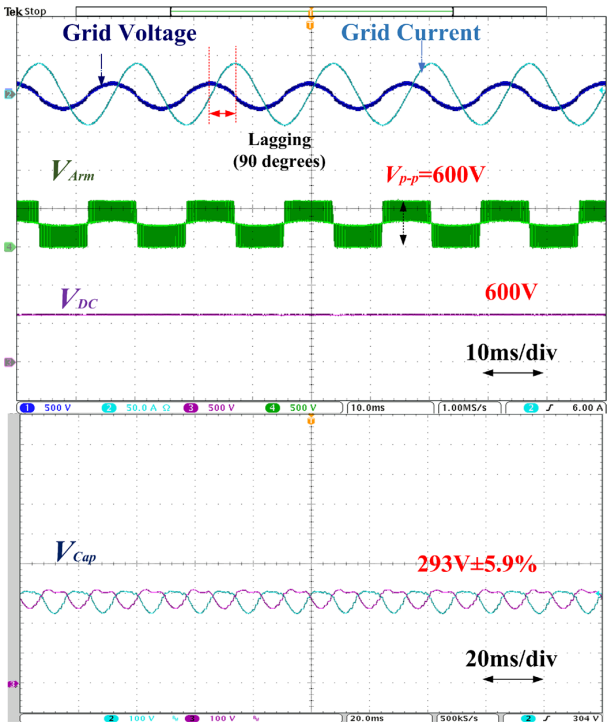

Figure 14. Experimental results of the reactive power/current control in the lagging mode: the grid voltage (500 V/div), grid current (50 A/div), arm voltage (500 V/div), DC-bus voltage (500 V/div) and capacitor voltage (100 V/div, from **top** to **bottom**).

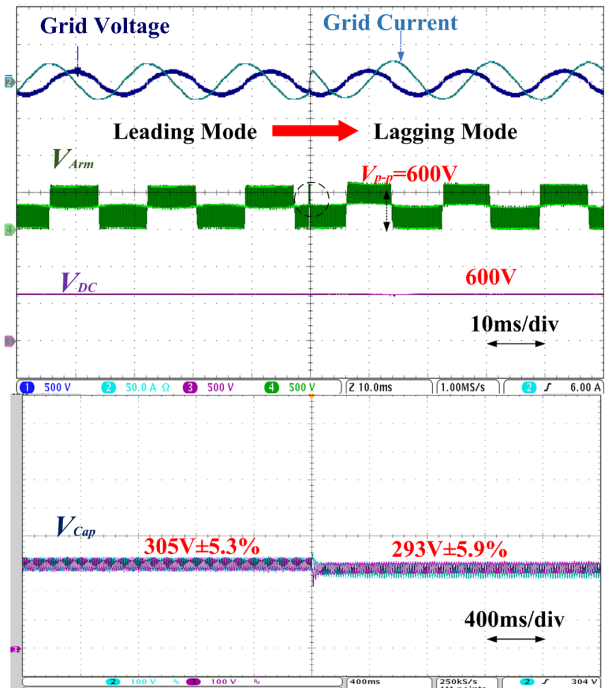

Figure 15. Dynamic response results from the leading to lagging mode: the grid voltage (500 V/div), grid current (50 A/div), arm voltage (500 V/div), DC-bus voltage (500 V/div), and capacitor voltage (100 V/div, from **top** to **bottom**).

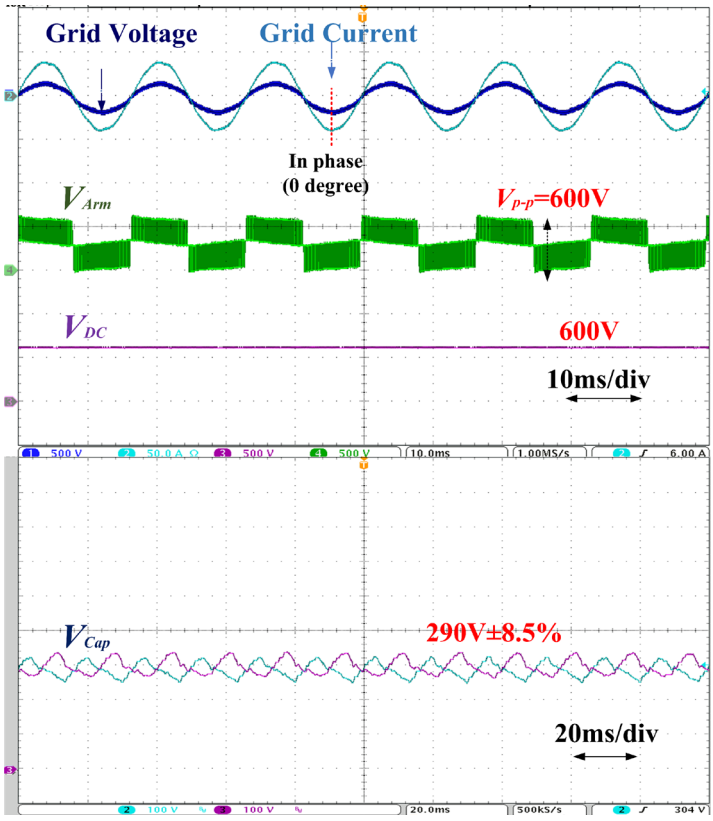

Figure 16. Experimental results of the active power/current control: the grid voltage (500 V/div), grid current (50 A/div), arm voltage (500 V/div), DC-bus voltage (500 V/div), and capacitor voltage (100 V/div, from **top** to **bottom**).

To investigate the transient response of the reactive power absorbed and supplied by MMC from the AC system, Figure 15 shows the corresponding experimental results. The rectifier step changed from the leading mode to the lagging mode. The results show that the grid current has a very quick response from the leading mode to the lagging mode with a high-quality waveshape. The SM capacitor voltages and DC-bus voltage are maintained at the given value after a small perturbation. No instability issues were observed during the whole process. Thus, the results in Figure 15 verify that the proposed strategy can provide a fast and robust response in terms of supplying or absorbing reactive power.

Figure 16 tests the active power/current control performance of the proposed sensorless control strategy. An active load is added on the DC output side. It can be seen that the grid current is exactly in phase with the grid voltage and has good sinusoidal characteristics, with an amplitude of 40 A. The upper and lower capacitor voltages are stable at approximately 300 V with fluctuations of around 10%. The DC-bus voltage is maintained at the given value of 600 V. Hence, the proposed sensorless control method works well for the active power/current control. It can effectively decouple the active and reactive current components with the accurate regulation capability of the current phase angle. Since the load on the output DC side can only absorb the active power from the AC grid, the condition of generating active power feeding the grid is not shown in this paper.

6. Conclusions

With conventional control methods, DC-bus voltage sensors must be installed for MMC-based rectifiers. This paper proposes a simple but effective control strategy for the MMC-based rectifier without implementing output DC-bus voltage sensors, resulting in reduced system cost/volume and increased reliability. The value of the output DC voltage is obtained through an evaluation algorithm. A closed-loop soft pre-charging scheme of the

MMC-based rectifier without a DC-bus voltage sensor is further presented. Validated by the simulated and testing results, the proposed method (1) effectively realizes controllable DC output voltage and has safe and rapid pre-charging of the MMC-based rectifier; (2) it has accurate and bidirectional active and reactive current control in both steady-state and dynamic conditions; (3) it makes the MMC-based rectifier function well even if the output DC-bus voltage sensor fails. Thus, the proposed method can advance MMC-based rectifier performance in applications of transportation electrification and renewable energy integration.

Author Contributions: Conceptualization, Z.K.; Data curation, Z.K.; Formal analysis, J.P.; Investigation, Z.K.; Methodology, J.P.; Software, Y.D.; Validation, Y.D.; Writing—original draft, J.P.; Writing—review and editing, Y.D. All authors have read and agreed to the published version of the manuscript.

Funding: This work was supported by the Natural Science Foundation of Chongqing under Grant CSTC2021JCYJ-MSXMX0871.

Data Availability Statement: Data is unavailable.

Conflicts of Interest: The authors declare no conflict of interest.

References

1. Ronanki, D.; Williamson, S.S. Modular multilevel converters for transportation electrification: Challenges and opportunities. *IEEE Trans. Transp. Electrif.* **2018**, *4*, 399–407. [CrossRef]
2. Ronanki, D.; Williamson, S.S. A simplified space vector pulse width modulation implementation in modular multilevel converters for electric ship propulsion systems. *IEEE Trans. Transp. Electrif.* **2019**, *5*, 335–342. [CrossRef]
3. Krastev, I.; Tricoli, P.; Hillmansen, S.; Chen, M. Future of electric railways: Advanced electrification systems with static converters for ac railways. *IEEE Electrif. Mag.* **2016**, *4*, 6–14. [CrossRef]
4. Ali, S.; Ling, Z.; Tian, K.; Huang, Z. Recent advancements in submodule topologies and applications of MMC. *IEEE J. Emerg. Sel. Top. Power Electron.* **2021**, *9*, 3407–3435. [CrossRef]
5. Pan, J.; Ke, Z.; Al Sabbagh, M.; Li, H.; Potty, K.A.; Perdikakis, W.; Na, R.; Zhang, J.; Wang, J.; Xu, L. 7-kV 1-MVA SiC-based modular multilevel converter prototype for medium-voltage electric machine drives. *IEEE Trans. Power Electron.* **2020**, *35*, 10137–10149. [CrossRef]
6. Ke, Z.; Pan, J.; Al Sabbagh, M.; Na, R.; Zhang, J.; Wang, J.; Xu, L. Capacitor voltage ripple estimation and optimal sizing of modular multi-level converters for variable-speed drives. *IEEE Trans. Power Electron.* **2020**, *35*, 12544–12554. [CrossRef]
7. Li, H.; Sun, Y.; Xie, S.; Xiong, W.; Su, M. Improved branch energy balance control for three-phase to single-phase modular multilevel converter for railway traction power supply. *IEEE Trans. Transp. Electrif.* **2022**, *9*, 87–98. [CrossRef]
8. He, X.; Peng, J.; Han, P.; Liu, Z.; Gao, S.; Wang, P. A novel advanced traction power supply system based on modular multilevel converter. *IEEE Access* **2019**, *7*, 165018–165028. [CrossRef]
9. Rodríguez, J.R.; Dixon, J.W.; Espinoza, J.R.; Pontt, J.; Lezana, P. PWM regenerative rectifiers: State of the art. *IEEE Trans. Ind. Electron.* **2005**, *52*, 5–22. [CrossRef]
10. Li, R.; Xu, L. A unidirectional hybrid HVDC transmission system based on diode rectifier and full-bridge MMC. *IEEE J. Emerg. Sel. Top. Power Electron.* **2021**, *9*, 6974–6984. [CrossRef]
11. Gong, Z.; Wu, X.; Dai, P.; Zhu, R. Modulated model predictive control for MMC-based active front-end rectifiers under unbalanced grid conditions. *IEEE Trans. Ind. Electron.* **2018**, *66*, 2398–2409. [CrossRef]
12. Steurer, M.M.; Schoder, K.; Faruque, O.; Soto, D.; Bosworth, M.; Sloderbeck, M.; Bogdan, F.; Hauer, J.; Winkelnkemper, M.; Schwager, L.; et al. Multifunctional megawatt-scale medium voltage dc test bed based on modular multilevel converter technology. *IEEE Trans. Transp. Electrif.* **2016**, *2*, 597–606. [CrossRef]
13. Liu, L.; Zhou, Z.; Dai, N.; Lao, K.W.; Song, Y. Interpolated phase-shifted PWM for harmonics suppression of multilevel hybrid railway power conditioner in traction power supply system. *IEEE Trans. Transp. Electrif.* **2022**, *8*, 898–908. [CrossRef]
14. Ma, F.; Xu, Q.; He, Z.; Tu, C.; Shuai, Z.; Luo, A.; Li, Y. A railway traction power conditioner using modular multilevel converter and its control strategy for high-speed railway system. *IEEE Trans. Transp. Electrif.* **2016**, *2*, 96–109. [CrossRef]
15. Liu, J.; Dong, D.; Zhang, D. Hybrid modular multilevel rectifier: A new high-efficient high-performance rectifier topology for HVDC power delivery. *IEEE Trans. Power Electron.* **2021**, *36*, 8583–8587. [CrossRef]
16. Liu, J.; Zhang, D.; Dong, D. Analysis of hybrid modular multilevel rectifier operated at nonunity power factor for HVDC applications. *IEEE Trans. Power Electron.* **2022**, *37*, 10642–10657. [CrossRef]
17. Debnath, S.; Qin, J.; Bahrani, B.; Saeedifard, M.; Barbosa, P. Operation, control, and applications of the modular multilevel converter: A review. *IEEE Trans. Ind. Electron.* **2014**, *30*, 37–53. [CrossRef]
18. Ji, S.; Huang, X.; Palmer, J.; Wang, F.; Tolbert, L.M. Modular multilevel converter (MMC) modeling considering submodule voltage sensor noise. *IEEE Trans. Power Electron.* **2021**, *36*, 1215–1219. [CrossRef]

19. LEM. Voltage Transducer LV 200-AW/2/6400. Available online: https://www.lem.com/en/product-list/lv-200aw26400 (accessed on 1 January 2023).
20. CHV-6KV-10KV. Available online: http://www.bjsse.com.cn/cn/productshow.asp?id=84 (accessed on 2 July 2021).
21. Wang, H.; Wang, H.; Wang, Z.; Zhang, Y.; Pei, X.; Kang, Y. Condition monitoring for submodule capacitors in modular multilevel converters. *IEEE Trans. Power Electron.* **2019**, *34*, 10403–10407. [CrossRef]
22. Wang, Z.; Zhang, Y.; Wang, H.; Blaabjerg, F. Capacitor condition monitoring based on the dc-side start-up of modular multilevel converters. *IEEE Trans. Power Electron.* **2020**, *35*, 5589–5593. [CrossRef]
23. Shi, X.; Liu, B.; Wang, Z.; Li, Y.; Tolbert, L.M.; Wang, F. Modeling, control design, and analysis of a startup scheme for modular multilevel converters. *IEEE Trans. Ind. Electron.* **2015**, *62*, 7009–7024. [CrossRef]
24. Das, A.; Nademi, H.; Norum, L. A method for charging and discharging capacitors in modular multilevel converter. In Proceedings of the IECON 2011—37th Annual Conference of the IEEE Industrial Electronics Society, Melbourne, VIC, Australia, 7–10 November 2011.
25. Tian, K.; Wu, B.; Du, S.; Xu, D.; Cheng, Z.; Zargari, N.R. A simple and cost-effective precharge method for modular multilevel converters by using a low-voltage DC source. *IEEE Trans. Power Electron.* **2016**, *31*, 5321–5329. [CrossRef]
26. Li, B.; Xu, D.; Zhang, Y.; Yang, R.; Wang, G.; Wang, W.; Xu, D. Closed-loop precharge control of modular multilevel converters during start-up processes. *IEEE Trans. Power Electron.* **2015**, *30*, 524–531. [CrossRef]
27. Xue, Y.; Xu, Z.; Tang, G. Self-start control with grouping sequentially precharge for the C-MMC-based HVDC system. *IEEE Trans. Power Deliv.* **2014**, *29*, 187–198. [CrossRef]